

See discussions, stats, and author profiles for this publication at: <https://www.researchgate.net/publication/231390633>

Calcium-Incorporated Mesoporous Aluminosilicates: Synthesis, Characterization, and Applications to the Condensation of Long-Chain Fatty Acid with Long-Chain Amine and Alcohol

ARTICLE *in* INDUSTRIAL & ENGINEERING CHEMISTRY RESEARCH · NOVEMBER 2009

Impact Factor: 2.59 · DOI: 10.1021/ie900641u

CITATIONS

11

READS

37

7 AUTHORS, INCLUDING:



Ayyamperumal Sakthivel

University of Delhi

77 PUBLICATIONS 1,584 CITATIONS

[SEE PROFILE](#)



Shing-Jong Huang

National Taiwan University

75 PUBLICATIONS 1,203 CITATIONS

[SEE PROFILE](#)



Shang-Bin Liu

Academia Sinica

163 PUBLICATIONS 3,570 CITATIONS

[SEE PROFILE](#)



Yoshihiro Sugi

Gifu University

252 PUBLICATIONS 3,088 CITATIONS

[SEE PROFILE](#)

Calcium-Incorporated Mesoporous Aluminosilicates: Synthesis, Characterization, and Applications to the Condensation of Long-Chain Fatty Acid with Long-Chain Amine and Alcohol

Ayyamperumal Sakthivel,^{†,‡} Kenichi Komura,[†] Shing-Jong Huang,[‡] Pei-Hao Wu,[§] Shang-Bin Liu,^{*,§} Yukichi Sasaki,[†] and Yoshihiro Sugi^{*,†}

Department of Materials Science and Technology, Faculty of Engineering, Gifu University, Gifu 501-1193, Japan,

Department of Chemistry, National Taiwan University, Taipei 10617, Taiwan, Institute of Atomic and Molecular Science, Academia Sinica, Taipei 10617, Taiwan, and Nanostructure Research Laboratory, Japan Fine Ceramics Centre, Nagoya 456-8587, Japan

A comprehensive study on a series of highly stable calcium containing mesoporous aluminosilicate molecular sieves (CaAlMMSH) having different acidic properties has been made by varying the Si/Ca ratio in synthesis gels. The structural, physical, and porous properties of these microporous/mesoporous composite materials were characterized by X-ray diffraction, N₂ adsorption/desorption isotherm measurements, solid-state ²⁷Al and ²⁹Si magic angle spinning NMR, and variable-temperature hyperpolarized ¹²⁹Xe NMR, Fourier transform infrared (FTIR) and diffuse reflectance FTIR spectroscopies. As compared to the parent AIMMSH materials, the incorporation of excessive amount of calcium tends to result in an overall increase in acid amount while at the expense of strong acid sites. The CaAlMMSH materials were found to have superior catalytic activities than AIMMSH in the amidation of palmitic acid with *N*-hexadecylamine. However, no significant enhancement in catalytic activity for the esterification of palmitic acid with cetyl alcohol was observed upon introducing calcium onto the AIMMSH materials. Such discrepancies were ascribed to variations in available acid sites and coking in the two different condensations reaction over the CaAlMMSH materials as catalysts.

1. Introduction

Microporous and mesoporous materials have been recognized as potential catalysts for many chemical transformations such as in petro-chemistry, petro-refining, organic synthesis, etc. Recently, several researchers have been interested in using porous solid acid catalysts for organic synthesis involving bulky molecules. While conventional porous aluminosilicate catalysts, such as zeolites, contain acid sites requisite for catalytic conversion of hydrocarbons, they also suffered from the steric limitation due to their smaller pore sizes (typically <1 nm), leading to insufficient activity due to the poor diffusion efficiency of bulky molecules. In this regard, mesoporous silicas,^{1,2} which possess large surface areas and tailorable pore sizes in the mesoporous range (typically 2–50 nm) may be advantageous for catalytic reaction involving bulkier organic molecules. However, the application of mesoporous materials has been limited because they only have weak overall acidity even when alumina is introduced as acidic components and they normally have amorphous wall characters, thus, low hydrothermal and mechanical stabilities.³

Recent advances in syntheses of novel mesoporous aluminosilicate materials with improved hydrothermal and mechanical stabilities mostly focus on incorporation of zeolite secondary building units (SBUs) on the mesopore walls.^{4–10} Among various mesoporous materials with zeolite framework charac-

teristics, highly stable mesoporous aluminosilicate molecular sieve (AlMMSH) materials exhibited the right niches for themselves as promising candidates for solid acid catalysts since they may be facilely synthesized without using sodium hydroxide and they exhibit improved hydrothermal stabilities.^{7–10}

Condensations of carboxylic acid with alcohols and amines are important and fundamental catalytic reactions in organic synthesis for advanced materials, medicines, agrochemicals, etc. Alkali metal ion-exchanged zeolites were found to be potential catalysts for the acylation of dimethylamine with acetic acid.¹¹ The proton-form of zeolite Y was also recognized as a potential catalyst for the amidation.¹² Nonetheless, these microporous zeolites have been adopted mostly for catalytic reactions involving relatively less bulky molecules. We report herein the syntheses and characterizations of calcium-containing AIMMSH materials (CaAlMMSH), and their catalytic performances in the condensation of palmitic acid with *N*-hexadecylamine and cetyl alcohol as typical examples involving bulky moieties.

2. Experimental Section

2.1. Synthesis of Calcium and Aluminum Containing MMSH Materials (CaAlMMSH). All chemicals, namely, colloidal silica (SiO₂; Ludox HS-40, Dupont), cetyltrimethylammonium bromide (CTMABr; Tokyo Kasei), polyoxyethylene(4)-lauryl ether (Brij-30; Tokyo Kasei), tetrapropylammonium hydroxide (TPAOH; Tokyo Kasei), aluminum nitrate nonahydrate (Al(NO₃)₃·9H₂O; Nakalai Tescque,) and calcium nitrate tetrahydrate (Ca(NO₃)₂·4H₂O; Nakalai Tescque) were used as received without further purification during the synthesis of the mesoporous materials. Typical molar composition of the gels: 5.0SiO₂/0.84CTMABr/0.16Brij-30/0.025Al₂O₃/*x*CaO/3.5TPAOH/400H₂O (where *x* is the fraction of mole of Ca introduce as CaO which is equal to 0.2, 0.125, 0.1, 0.066, 0.05,

* To whom correspondence should be addressed. (Y.S.) Tel.: +81-58-293-2597. Fax: +81-58-293-2653. E-mail: ysugi@gifu-u.ac.jp. (S.-B.L.) Tel.: +886-2-23668230. Fax: +886-2-23620200. E-mail: sbliu@sinica.edu.tw.

[†] Gifu University.

[‡] National Taiwan University.

[§] Academia Sinica.

[¶] Japan Fine Ceramics Centre.

^{||} Current address: Reliance Industries Limited, R&D Vadodara Manufacturing Division, Vadodara, Gujarat, India.

and 0 for Si/Ca ratios of 25, 40, 50, 75, 100, and ∞ , respectively) were prepared according to the literature procedures.^{7–9} In brief, a micellar solution of surfactants was first prepared by mixing CTMABr and Brij-30 with 30 mL of distilled water. Then the colloidal silica solution (40 wt %) was added followed by stirring the resultant mixture for about 30 min. Subsequently, an appropriate amount (43.75 g) of 1 M TPAOH solution was added into the gel under stirring condition for about 1 h. An appropriate amount of aluminum source ($\text{Al}(\text{NO}_3)_3 \cdot 9\text{H}_2\text{O}$) was dissolved in 5 mL of water, and was added dropwise into the aforementioned synthesis gel under stirring for an additional 1 h. The gel was allowed to crystallize under hydrothermal conditions at 373 K for 2 d. Then, the resultant gel was brought down to room temperature while the pH was adjusted to 10.5 using 6 M acetic acid solution, followed by an additional crystallization procedure for another 2 d at 373 K. Finally, a known amount of calcium source ($\text{Ca}(\text{NO}_3)_2 \cdot 4\text{H}_2\text{O}$) was added into the synthesis gel, and the gel mixture was allowed to crystallize for an additional 5 d to incorporate calcium onto the framework. It is noted that the calcium source was introduced after the mesoporous solid was formed because the formation of mesoporous phase may be disturbed if calcium is introduced during the initial stage of crystallization. The as-synthesized materials were calcined in air at 823 K for 6 h. Resultant samples with a fixed Si/Al ratio of 100 are designated as $\text{Ca}(x)\text{AlIMMSH}$, where x represents the Ca/Si ratio ranging from 25 to 100. For comparison purpose, an AlMCM-48 sample was also prepared by a similar procedure as CaAlIMMSH materials, except that sodium hydroxide was used as base instead of TPAOH.

2.2. Characterization of CaAlIMMSH Materials. Powder X-ray diffraction (XRD) was measured by a Shimadzu XRD-6000 diffractometer with $\text{K}\alpha$ radiation ($\alpha = 1.5418 \text{ \AA}$). Elemental analysis was performed using an inductively coupled plasma (ICP) spectrophotometer (JICP-PS-1000 UV; Leeman Laboratories, Inc.) after the destruction of the samples by potassium carbonate. Nitrogen adsorption/desorption isotherm measurements were carried out on a Belsorp 28SA apparatus (Bel, Japan). Transmission electron microscopy (TEM) images were observed under low dose conditions using a JEOL JEM-2000FXII microscope at 200 kV. The ^{27}Al and ^{29}Si magic angle spinning (MAS) NMR spectra were recorded at ambient temperature under MAS by using 4 mm diameter zirconia rotors spinning at 15 kHz for ^{27}Al and at 5 Hz for ^{29}Si on an ECA-500 NMR spectrometer (JEOL Ltd.). Ammonia temperature programmed desorption (NH_3 -TPD) experiments were conducted on a TPD-66 apparatus (Bel Japan). Prior to each run, the catalyst was first evacuated at 673 K for 1 h, then, ammonia was adsorbed at 373 K followed by further evacuation for 1 h. For each NH_3 -TPD measurement, the sample was heated from 373 to 983 K with a rate of 10 K/min under a helium stream. Thermal gravimetric analyses (TGA) were carried out by using a Shimadzu DTG-50 analyzer at a ramping rate of 10 K/min under an air stream.

All IR experiments were conducted on a Bruker Optik IFS-28 spectrometer. Prior to each run, compressed sample (in form of a self-supporting wafer, ca. 6 mg/cm²) placed in the IR cell (with ZnSe windows) was first subjected to evacuation treatment at 673 K for 3 h. Typically, 16 repeated scans were accumulated for each FTIR and DRIFT spectra.

2.3. Variable-Temperature Hyperpolarized ^{129}Xe NMR Experiments. To find out the effects of incorporating calcium on the pore structure of the CaAlIMMSH materials, the porosity and surface properties of the samples were studied by variable-temperature (VT) hyperpolarized ^{129}Xe NMR spectroscopy;

detailed experimental procedures can be found elsewhere.¹³ In brief, HP ^{129}Xe gas was fabricated by an optical pumping setup consisting of a diode laser with a wavelength of 794.8 nm (Coherent; FAP-30; maximum power 30 W), a circular polarizer unit (Coherent; CPU), a mass flow controller (Matheson; 8272-0413), and a home-designed optical pumping cell. The optical pumping station was placed in the fringe field (ca. 200 G) of the superconducting magnet. The spin-exchange optical pumping process was facilitated by introducing a gas mixture (97% He, 1% N_2 , and 2% natural Xe) into the pumping cell (containing ca. 1 g of Rb metal) maintaining at a constant pressure (4 atm), temperature (423 K), and gas flow rate (ca. 100 scc/min) while subjecting to irradiation by a left-circularly polarized light source. As a result, an estimated polarization of ca. 2.4% for HP ^{129}Xe gas was achieved, corresponding to an overall enhancement in signal sensitivity of ca. 3500. The optical pumping unit was connected to a home-designed NMR sample cell, such that the fabricated HP ^{129}Xe gas can be continuously delivered (via 1/16 in. Teflon tubing) to the sample under ambient pressure, corresponding to a Xe partial pressure of ca. 15.2 Torr. It is noteworthy that the presence of He and N_2 in the gas mixture has no significant effect on the observed HP ^{129}Xe NMR spectra. Prior to each NMR run, ca. 0.5 g of the sample was compressed under 100 MPa pressure, then, crashed into small pellets before being subjected to dehydration treatment (at 423 K for 12 h) under a vacuum (<10⁻⁴ Torr). All HP ^{129}Xe NMR spectra were acquired on a Bruker Avance 300 NMR spectrometer at a Larmor frequency of 83.012 MHz using a single-pulse sequence with a pulse angle of ca. 15° and a recycle delay of 5 s. Typically, spectra with excellent sensitivity can be attained by accumulating about 64–256 free-induction-decay signals. VT experiments were conducted in the temperature range of 150–298 K, as limited by the existing facility. Sample temperature was calibrated using the ^{209}Pb NMR signal of solid $\text{Pb}(\text{NO}_3)_2$. The ^{129}Xe NMR chemical shift (CS) was referenced to that of xenon gas extrapolated to zero pressure.

2.4. Amidation and Esterification. The amidation of palmitic acid was carried out in mesitylene medium using the procedure given below: palmitic acid (0.3846 g; 1.5 mmol), *N*-hexadecylamine (0.3622 g; 1.5 mmol), 30 mL mesitylene as solvent and a catalyst (0.05 g) were placed in a 100 mL round bottle flask. The reaction was carried out by initial agitation at 150 °C for 6 h, then, the reactor was cooled to room temperature, and the solid products were filtered and washed repeatedly with ethanol/chloroform mixture. The products were analyzed by gas chromatography (Shimadzu gas chromatograph 14A using capillary columns Ultra-1 (25 m × 0.3 mm and 0.32 μm thick layer)). The conversion was expressed on the basis of palmitic acid consumed. Similar procedures were also adopted for esterification except that the reactant of cetyl alcohol (0.3637 g; 1.5 mmol), instead of *N*-hexadecylamine, was used.

3. Results and Discussion

3.1. Synthesis and Characterization of CaAlIMMSH. It is well-known that the mesoporous materials originally developed by Mobile group have some drawbacks, such as weak acidity and lack of hydrothermal and mechanical stabilities, etc.³ In this context, the syntheses of highly stable mesoporous aluminosilicate molecular sieves (AlIMMSH) with characteristics of microporous zeolitic walls, developed by Liu and co-workers,⁷ open new aspects as catalysts for organic synthesis due to substantial improvements in acidity and hydrothermal/mechanical stabilities.⁸ Nevertheless, a more delicate control of such microporous/mesoporous composite catalysts with desirable

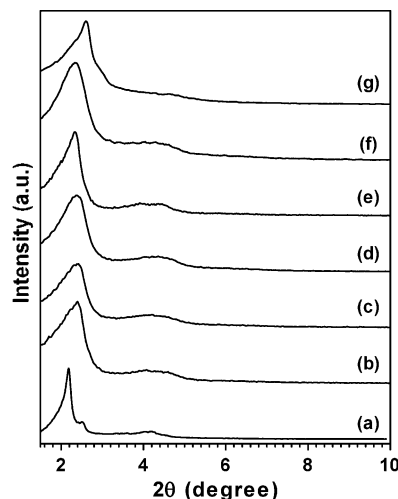


Figure 1. XRD patterns of (a) AIMCM-48, (b) AIMMSH, (c) Ca(100)AIMMSH, (d) Ca(75)AIMMSH, (e) Ca(50)AIMMSH, (f) Ca(40)AIMMSH, and (g) Ca(25)AIMMSH materials.

acidic properties, for example, by incorporating heteroatoms, deserves further investigations in terms of their catalytic performances for specific reactions. This study aims to explore the influences of calcium on the acidity of the catalysts by its incorporation onto the AIMMSH materials. Calcium was introduced into the synthesis gel after the self-assembly of AIMMSH mesoporous arrays.

As shown in Figure 1, all XRD patterns of the calcined AIMCM-48, AIMMSH, and CaAIMMSH materials with different Si/Ca ratios exhibit a main characteristic peak corresponding to the (211) plane along with a broad shoulder peak from the (220) plane at 2θ angles of about 2.3° and 3.0° , respectively. These peaks, together with the sextet pattern observed between 2θ angles of $3\text{--}6^\circ$, represent the typical structural characteristics of the AIMCM-48 type (including AIMMSH) materials.^{7\text{--}9} The broadening of the main peak and the weak shoulder peaks are due to the existence of Al^{3+} species in the framework as well as calcium in the CaAIMMSH materials.

Table 1 summarizes the physicochemical properties of CaAIMMSH and AIMMSH materials. Elemental analyses by ICP reveal that the Si/Al and Si/Ca ratios remain practically the same as that of starting synthesis gels, indicating the effective incorporation of aluminum and calcium into the mesoporous arrays.^{9,14,15} The N_2 adsorption/desorption curves of CaAIMMSH materials shown in Figure 2 exhibit the typical type IV isotherms according to the IUPAC,¹⁶ and characteristics for mesoporous solids. Typically, well-defined inflections are observed for all samples at the relative pressure (p/p_0) of $0.3\text{--}0.4$, which are ascribed due to capillary condensation of N_2 inside the primary mesopores. In addition, the surface areas, pore-sizes, and pore volumes of various samples show typical characteristics of mesoporous materials. The pore volume decreased with increasing calcium content in CaAIMMSH materials, which indicates

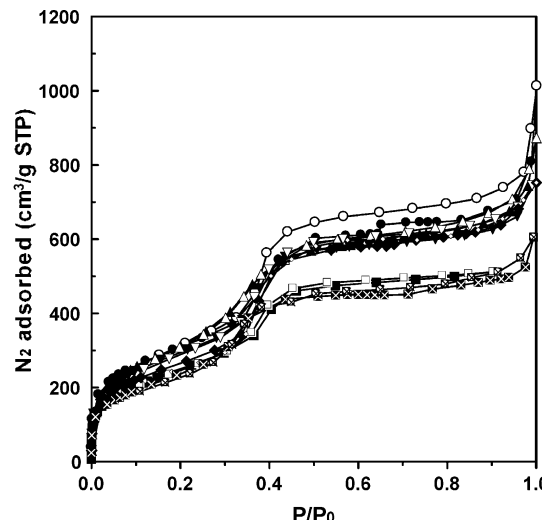


Figure 2. N_2 adsorption/desorption isotherms (at 77 K) of AIMMSH (■, □), Ca(100)AIMMSH (●, ○), Ca(75)AIMMSH (▲, △), Ca(50)AIMMSH (▼, ▽), Ca(40)AIMMSH (◆, ◇), Ca(25)AIMMSH (filled box with ×, empty box with ×) materials.

that the incorporated calcium is located mostly in the mesoporous channels.

The TEM images of AIMMSH, Ca(100)AIMMSH, and Ca(25)AIMMSH are shown in Figure 3. It is further confirmed that all the materials possess uniform pores. The slight disorder observed on calcium-containing MMSH materials is most likely due to the introduction of the heteroatom (*i.e.*, Ca) onto the mesoporous aluminosilicate frameworks.^{7,19}

The porosity and surface properties of the samples were further characterized by the continuous-flow HP ^{129}Xe NMR technique.^{7,13,17,18} Both spectral sensitivity and the ^{129}Xe chemical shift (CS) from the conventional ^{129}Xe NMR spectra are strongly dependent on the Xe–Xe interactions (*i.e.*, Xe loading) present in the sample. On the other hand, the CSs observed by HP ^{129}Xe NMR spectra reflect predominately the interactions between the Xe atom and the internal surfaces of the porous adsorbents because HP ^{129}Xe NMR experiments are conducted at dilute Xe loading at constant temperature.^{13,18} Accordingly, different porous environments can be inferred from the variations in the ^{129}Xe chemical shift at various temperatures. Figure 4 shows the HP ^{129}Xe NMR spectra of Ca(100)AIMMSH, Ca(100)AIMCM-48, AIMCM-48 at 180 K, AIMMSH, and mixtures of ZSM-5 with AIMCM-48 materials at 180 K. In accordance with our previous study,⁷ the HP ^{129}Xe NMR spectra observed for the AIMMSH sample at low temperatures (≤ 220 K) showed multiple resonances in the downfield relative to the dilute Xe gas at 0 ppm (see Figure S1 in Supporting Information). For example, the spectrum obtained for the AIMMSH sample in Figure 4 clearly reveals three overlapped resonance peaks at 131.4, 112.1, and 100.5 ppm. The former peak with the highest CS may be ascribed to Xe adsorbed in micropores of the zeolitic frameworks, whereas the other two peaks should

Table 1. Physicochemical Properties of AIMMSH and CaAIMMSH Materials

sample	Si/Al	Si/Ca	S_{BET} (m^2/g)	W_{BJH}^a (nm)	V_{meso} (cm^3/g)	acid mount (mmol/g)
AIMMSH	108		879	2.74	1.63	0.310
Ca(100)AIMMSH	103	94	1104	3.18	1.28	0.302
Ca(75)AIMMSH	112	74	1091	2.74	1.26	0.390
Ca(50)AIMMSH	106	48	1051	3.0	1.16	0.344
Ca(40)AIMMSH	116	41	951	2.96	1.21	0.236
Ca(25)AIMMSH	105	28	812	2.74	0.95	0.252

^a W_{BJH} = Pore size distribution.

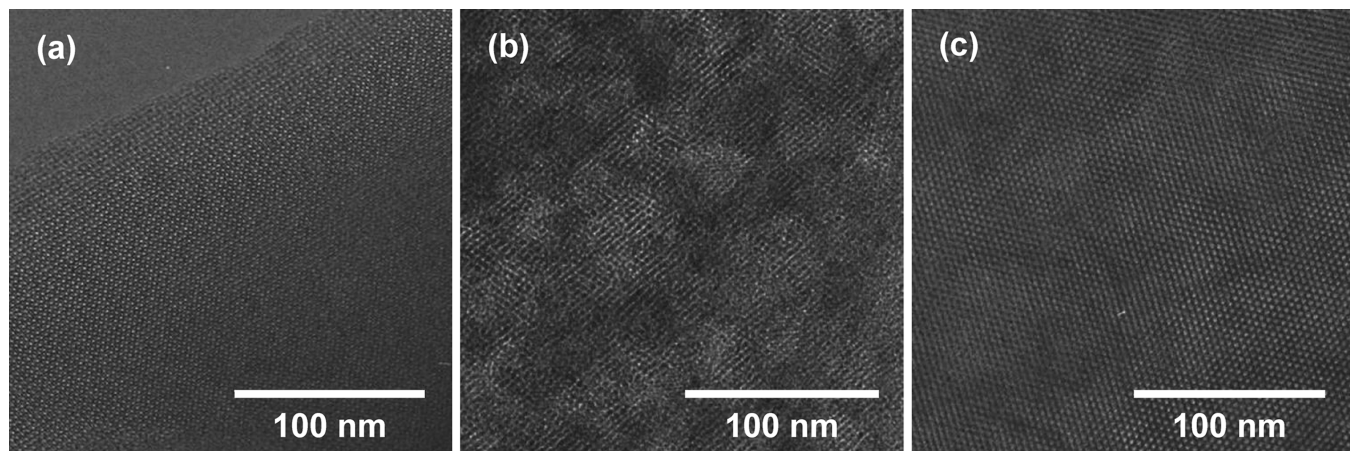


Figure 3. TEM images of (a) AIMMSH, (b) Ca(100)AIMMSH, and (c) Ca(25)AIMMSH materials.

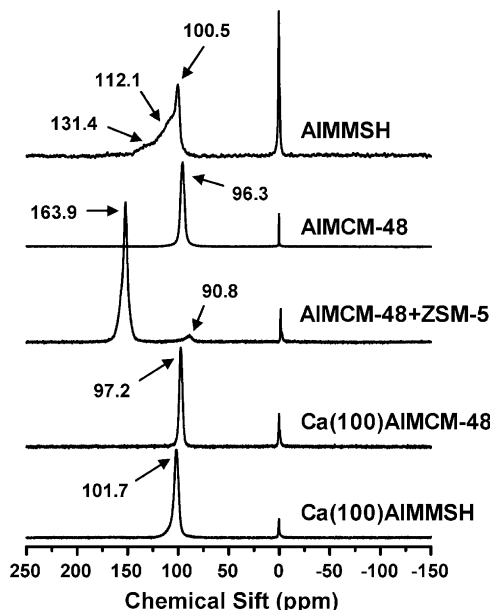


Figure 4. HP ^{129}Xe NMR spectra of various materials obtained at 180 K.

arise from two different types of mesopores in the AIMMSH sample.⁷ On the other hand, the spectra obtained from the conventional AIMCM-48 (Supporting Information, Figure S2) reveal only a main resonance peak at 96.3 ppm due to Xe in mesoporosity, whereas those of a (1:1) physical mixture of AIMCM-48 and ZSM-5 (Supporting Information, Figure S3) reveal two distinct peaks at 163.9 and 90.8 ppm responsible for Xe in micropores (ZSM-5) and mesoporous (AIMCM-48). The above observations clearly indicate that the AIMMSH material indeed consists of mesoporosities with microporous (zeolite) walls, which is in good agreement with HP ^{129}Xe NMR results obtained from similar meso/microcomposite materials.¹⁹

Unlike AIMMSH, HP ^{129}Xe spectra of the Ca(100)AIMMSH and Ca(100)AIMCM-48 samples at 180 K reveal only a singlet at 101.7 ppm (in addition to the gaseous Xe peak at ca. 0 ppm) arising from Xe adsorbed in mesopores. As can be referred from the VT-HP ^{129}Xe NMR spectra (Supporting Information, Figures S4 and S5), a gradual increase in chemical shift (CS) with decreasing temperature due to progressive condensation of Xe in the mesopores is observed for both Ca(100)AIMMSH and Ca(100)AIMCM-48. As such, the peak observed for Ca(100)AIMMSH at 101.7 ppm (at 180 K) should be corresponding to the mesoporous channel. There is no additional peak appeared even

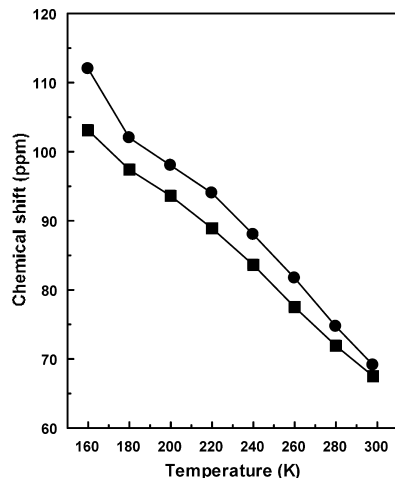


Figure 5. Variations of ^{129}Xe chemical shift with temperature for Ca(100)AIMMSH (●) and Ca(100)AIMCM-48 (■) materials.

at very low temperature. From these results, it is conclusive that the incorporation of calcium into AIMMSH prevents access of xenon to most of micropores on the pore walls, leading to a fast-exchange of Xe between calcium occupied zeolite SBUs and mesopores in the NMR time-scale, thus, the presence of a singlet resonance in CaAIMMSH. The observed higher CS values for Ca(100)AIMMSH than Ca(100)AIMCM-48 at the same temperature (Figure 5) indicates stronger interactions between Xe and the rougher pore surfaces containing zeolite SBUs on the walls of the former materials.

FT-IR spectra of AIMMSH and CaAIMMSH materials (Figure 6) revealed that, along with typical vibration bands arising from the aluminosilicates framework, an additional weak band at ca. 545 cm^{-1} was observed in both samples, which appears in ZSM-5 as stronger absorbance. This band, which is absent in conventional AIMCM-48, is a characteristic of zeolite SBUs. A somewhat broader band (compared to ZSM-5) was also observed for CaAIMMSH and AIMMSH thus confirms the presence of zeolite SBUs on the walls of the mesoporous channels.^{5–7,19}

Figure 7 shows the ^{27}Al and ^{29}Si MAS NMR spectra of CaAIMMSH and AIMMSH materials. All ^{27}Al spectra exhibit only a symmetrical peak at ca. 55 ppm. These results reveal that the CaAIMMSH and AIMMSH materials were free of extra-framework (octahedral) Al species and that a majority of the Al species is tetrahedral coordinated even upon an extensive introduction of calcium, such as in Ca(25)AIMMSH ($\text{Si}/\text{Ca} = 28$; see Table 1). No additional signal was observed in the ^{27}Al

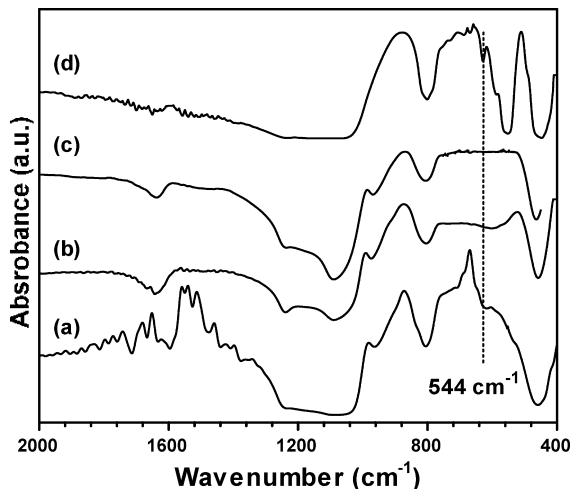


Figure 6. FT-IR spectra of (a) Ca(100)AlMMSH, (b) AlMMSH, (c) AlMCM-48, and (d) H-ZSM-5.

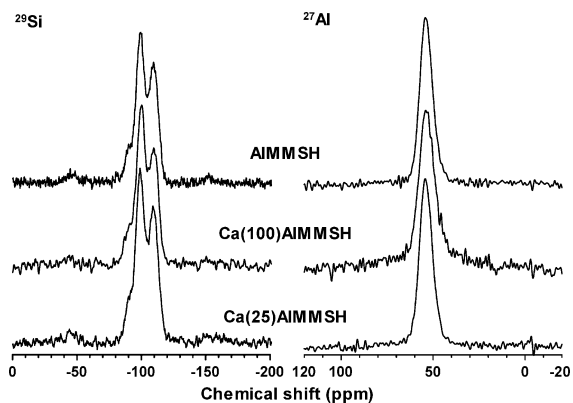


Figure 7. Solid-state ^{27}Al and ^{29}Si MAS NMR spectra of AlMMSH, Ca(100)AlMMSH, and Ca(25)AlMMSH materials.

NMR spectra other than the peak at 55 ppm, which clearly indicates the absence of any segregated CaO species nearby to the framework Al.²⁰ Furthermore, the ^{29}Si spectra observed for all samples ($\text{Si}/\text{Al} \approx 100$) are in close resemblance among the samples, which show similar silica environments. The slight increases and broadening of Q² (at ca. -90 ppm) and Q³ (at ca. -110 ppm) signals observed for CaAlMMSH upon increasing calcium content compared to the ^{29}Si spectrum of AIMMSH are ascribed to the influences of calcium on the environments of the adjacent Si atoms.²¹ It has been reported earlier that calcium aluminosilicates prepared under hydrothermal synthesis conditions with the molar gel pH in the range of 10–12.5 contained $\text{Ca}(\text{OH})_2$ species,^{22,23} however, after a postsynthesis treatment, calcium tends to occupy on the silicates and aluminosilicates as $\text{Ca}(\text{OH})^+$ species, as confirmed by earlier diffuse reflectance FTIR (DRIFT) studies.^{23,24} A sharp signal around 3740 cm^{-1} in DRIFT spectra of AlMCM-48, AlMMSH, CaAlMCM-48, and CaAlMMSH indicates the presence of Brønsted acid sites (Figure S6). CaAlMMSH and CaAlMCM-48 materials showed much sharper signal with a broadening of signal in the range of $3600\text{--}3550\text{ cm}^{-1}$; such a broadening arises from $\text{Ca}(\text{OH})^+$ species.^{23,24} However, the exact nature of calcium in the framework of CaAlMMSH materials remains unclear, and hence pending for further studies.

NH_3 -TPD profiles of CaAlMMSH and AlMMSH materials are shown in Figure 8. It is clear that the TPD profile of AlMMSH reveals three desorption peaks with maximum desorption temperatures at ca. 210, 320, and 560 °C corresponding

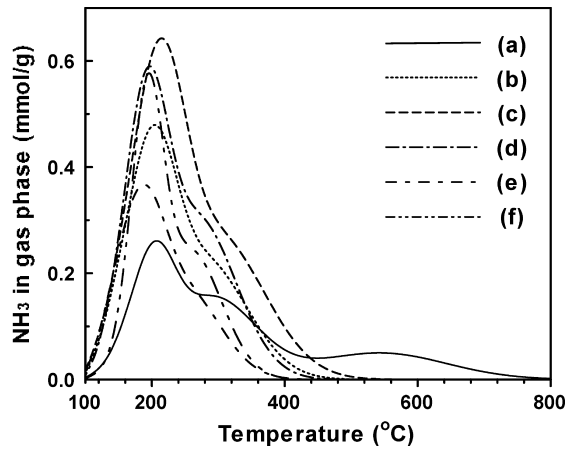


Figure 8. NH_3 -TPD profiles of (a) AIMMSH, (b) Ca(100)AlMMSH, (c) Ca(75)AlMMSH, (d) Ca(50)AlMMSH, (e) Ca(40)AlMMSH, and (f) Ca(25)AlMMSH materials.

to weak, moderate, and strong acid sites, respectively. Because the ^{27}Al MAS NMR spectrum of AIMMSH (Figure 7) reveals the absence of octahedral Al^{3+} species, the latter desorption peak at higher temperatures as 560 °C is the acid sites associated with the Lewis acidity of extra-framework octahedral Al^{3+} species as previously assigned.²⁵ As such, this high temperature desorption peak most likely arose from tetrahedral Al species (bridging hydroxyls of the Brønsted acidity) in association with adjacent silanols, as proposed by Niwa and co-workers.²⁶ The medium temperature desorption peak at 320 °C responsible for strong acid sites for CaAlMMSH diminishes by introducing calcium onto AlMMSH. Meanwhile, the amount of NH_3 desorbed tends to first increase with increasing calcium content (up to $\text{Si}/\text{Ca} \approx 75$), and then, gradually decrease by further increasing the calcium content. This is accompanied by a progressive decrease in maximum desorption temperatures responsible for the weak and moderate acid sites upon increasing the amount of incorporated calcium. In other words, the variations in acid amount and strength associated with the weak and moderate acid sites are seemingly decreased upon dosage of calcium in CaAlMMSH materials at the expense of the strongest acid sites observed for AIMMSH. It is hypothesized that the calcium ions tend to occupy the strong acid sites via ion-exchange processes, leading to the decrease in the desorption peak associated with the strongest (Brønsted) acid sites in the NH_3 -TPD profile. Okabe et al.²⁷ reported that the introduction of a small amount of calcium onto ZSM-5 led to formation of weak acid sites, and they suggested that calcium is somewhat incorporated in the silicate lattice. The introduction of a small amount of calcium into the CaAlMMSH framework should also provoke formation of additional weak acid sites, resulting in an overall increase in acidity. However, the excess calcium may be presented either as $\text{Ca}(\text{OH})^+$ or calcium oxide upon a progressive increase in calcium content, which in turn may be deposited on the acid sites, leading to a progressive decrease in acid strength.

3.2. Catalytic Properties of CaAlMMSH Materials in Condensation of Long-Chain Fatty Acid with Long-Chain Amine and Alcohol. The CaAlMMSH and AlMMSH materials were applied as catalysts for the condensations of long-chain fatty acid with long-chain amine and alcohol: the amidation of palmitic acid with *N*-hexadecylamine and the esterification of palmitic acid with cetyl alcohol. The typical results are shown in Table 2. It is clear that these microporous/mesoporous composite aluminosilicate materials are highly potential catalysts for the amidation, leading to the typical yield of *N*-hexadecyl-

Table 2. Condensation of Palmitic Acid with *N*-Hexadecylamine and Cetyl Alcohol over AIMMSH and CaAIMMSH Materials as Catalysts^a

catalysts	yield of amide (%)	yield of ester (%)
without catalyst	10	3.0
AIMMSH	58	8.0
Ca(100)AIMMSH	65	7.4
Ca(75)AIMMSH	69	5.0
Ca(50)AIMMSH	54	8.8
Ca(40)AIMMSH	56	5.7
Ca(25)AIMMSH	50	2.8

^a Reaction conditions: palmitic acid 0.3846 g (1.5 mmol); *N*-hexadecylamine 0.3622 g (1.5 mmol) or cetyl alcohol 0.3637 g (1.5 mmol); catalyst, 50 mg; solvent, mesitylene, 30 mL; temperature, 150 °C; period, 6 h.

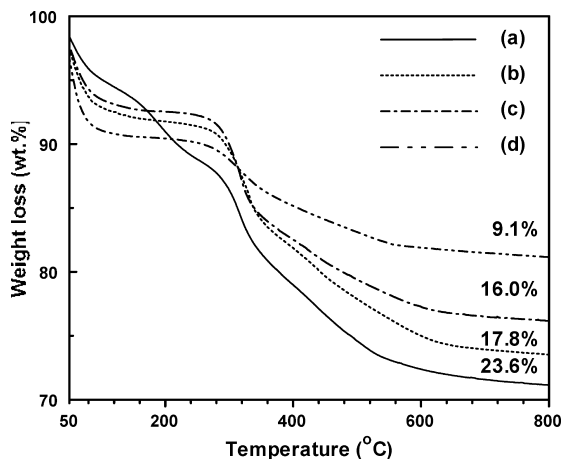


Figure 9. TGA profiles of (a) AIMMSH, (b) Ca(100)AIMMSH, (c) Ca(50)AIMMSH, and (d) Ca(25)AIMMSH materials.

hexadecanamide of 50–70%. In particular, CaAIMMSH materials contained a smaller amounts of calcium ($\text{Si/Ca} \geq 75$) and have superior catalytic performances compared to those with excessive amount of incorporated calcium. Based on the $\text{NH}_3\text{-TPD}$ results and previous studies on calcium silicates,²⁷ the presence of a small amount of calcium tends to yield considerable weak acidic sites, leading to an overall increase in total acidity (Table 1) and hence resulting in a superior yield for the amidation. However, an increase of a small amount of calcium content on CaAIMMSH ($\text{Si/Ca} = 50$; Ca(50)AIMMSH) results in more weak acid sites (see Figure 8), which leads to reduction of overall amide yield. Further, increasing the amount of incorporated calcium (Ca(40)AIMMSH and Ca(25)AIMMSH) leads to the formation of hydroxide (Ca(OH)^+) and oxide (CaO) species, which may occupy the acid sites, reducing the acid sites (see Table 1), and subsequently reducing the amide yield.

Although the CaAIMMSH and AIMMSH catalysts gave similar level of amide yields; TGA profiles showed that the amount of organic and carbonaceous deposits presented in the corresponding spent catalysts decreases with increasing calcium content (Figure 9). This may be due to the effective suppression of strong acid sites (Figure 8), and hence, the reduction in the formation of carbonaceous deposits. These observations indicate that secondary reactions may be largely retarded by introducing a proper amount of calcium onto AIMMSH materials. The presence of a small amount of calcium was found to enhance the catalytic activity in the amidation. On other hand, these CaAIMMSH and AIMMSH materials are not suitable for the esterification of palmitic acid with cetyl alcohol (Table 2). The discrepancies in catalytic performances observed in amidation and esterification seem to be dictated by the interactions of

amine and alcohol against acid sites. For the amidation, the amines can be activated more easily upon adsorption on the acid sites, followed by subsequent interactions with fatty acid to form amide. However, the acid sites present on CaAIMMSH and AIMMSH catalysts are apparently not strong enough for the activation of alcohols, resulting in lower product yields in the esterification. This may be realized by the effect of adsorbed water, which tends to deactivate acid sites in the esterification but has practically no influence in the amidation. The exact nature and role of calcium in CaAIMMSH materials on the catalysis remain unclear, and further researches are necessary to clarify the details of the aforementioned phenomena observed.

4. Conclusions

A series of calcium containing mesoporous aluminosilicate materials (CaAIMMSH) with zeolitic walls were synthesized, characterized, and applied as catalysts for the condensation of fatty acid with amine and alcohol. The XRD and N_2 adsorption/desorption isotherm measurements confirmed the mesoporous nature of the materials. The presence of zeolite secondary building units (SBUs) on the pore walls is confirmed from the downfield shift for CaAIMMSH compared to AIMMSH in the HP ^{129}Xe NMR spectra, which is due to the occurrence of stronger interactions between Xe and the surfaces of the mesoporous channels. ^{29}Al and ^{27}Si MAS NMR spectra indicate that the presence of calcium in the synthesis gel is not influenced on the framework tetrahedral aluminum. The incorporated calcium species were found to present not only as ion-exchange cations on the strong acid sites but also as the form of CaO on the surface silanol groups of the mesoporous channels.

The CaAIMMSH materials exhibit high catalytic performances for the amidation of palmitic acid with *N*-hexadecylamine at moderate reaction conditions. These observations were ascribed to the presence of small amount of calcium on AIMMSH materials, which effectively hinder the deposition of organic reactants/products and formation of carbonaceous residues. However, they are less active for esterification of palmitic acid with cetyl alcohol.

Acknowledgment

Support of this work by the Japan Society for the Promotion of Science (Grant-in-Aid for Scientific Research (B) 1931006) and National Science Council, Taiwan (NSC95-2113-M-001-040-MY3), are gratefully acknowledged. A. Sakthivel is grateful to the JSPS for the postdoctoral fellowship.

Note Added after ASAP Publication: After this paper was published ASAP November 9, 2009, some corrections were made to the text; the corrected version was reposted November 12, 2009.

Supporting Information Available: Figures S1–S5. Variable-temperature (VT) hyperpolarized (HP) ^{129}Xe NMR spectra of AIMMSH, AIMCM-48, 1:1 physical mixture of AIMCM-48 and ZSM-5, Ca(100)AIMCM-48, and Ca(100)AIMMSH. Figure S6. DRIFT spectra of Ca(100)AIMMSH, Ca(100)AIMCM-48, AIMMSH, and AIMCM-48. This material is available free of charge via the Internet at <http://pubs.acs.org>.

Literature Cited

- Kresge, C. T.; Leonowicz, M. E.; Roth, W. J.; Vartuli, J. C.; Beck, J. S. Ordered mesoporous molecular sieves synthesized by a liquid-crystal template mechanism. *Nature* **1992**, *359*, 710–712.

- (2) Beck, J. S.; Vartuli, J. C.; Roth, W. J.; Leonowicz, M. E.; Kresge, C. T.; Schmitt, K. D.; Chu, C. T.-W.; Olson, D. H.; Sheppard, E. W.; McCullen, S. B.; Higgins, J. B.; Schlenker, J. L. A new family of mesoporous molecular sieves prepared with liquid crystal templates. *J. Am. Chem. Soc.* **1992**, *114*, 10834–10843.
- (3) Corma, A. From microporous to mesoporous molecular sieve materials and their use in catalysis. *Chem. Rev.* **1997**, *97*, 2373–2420.
- (4) Zhang, Z.; Han, Y.; Zhu, L.; Wang, R.; Yu, Y.; Qiu, S.; Zhao, D.; Xiao, F. S. Strongly acidic and high-temperature hydrothermally stable mesoporous aluminosilicates with ordered hexagonal structure. *Angew. Chem., Int. Ed.* **2001**, *40*, 1258–1262.
- (5) Liu, Y.; Pinnavaia, T. J. Aluminosilicate mesostructures with improved acidity and hydrothermal stability. *J. Mater. Chem.* **2002**, *12*, 3179–3190.
- (6) On, D. T.; Kaliaguine, S. Ultrastable and highly acidic, zeolite-coated mesoporous aluminosilicates. *Angew. Chem., Int. Ed.* **2002**, *41*, 1036–1040.
- (7) Sakthivel, A.; Huang, S. J.; Chen, W. H.; Lan, Z. H.; Chen, K. H.; Lin, H. P.; Mou, C. Y.; Liu, S. B. Direct synthesis of highly stable mesoporous molecular sieves containing zeolite building units. *Adv. Funct. Mater.* **2005**, *15*, 253–258.
- (8) Sakthivel, A.; Chen, W. H.; Liu, S. H.; Huang, S. J.; Lo, A. Y.; Hsu, Y. H.; Lin, S. D.; Mou, C. Y.; Liu, S. B. Acidity and catalytic behaviors of ordered mesoporous aluminosilicate materials containing zeolite building units. *Catal. Lett.* **2006**, *108*, 173–178.
- (9) Sakthivel, A.; Nakamura, R.; Komura, K.; Sugi, Y. Esterification of glycerol by lauric acid over aluminium and zirconium containing mesoporous molecular sieves in supercritical carbon dioxide medium. *J. Supercrit. Fluids* **2007**, *42*, 219–225.
- (10) Sakthivel, A.; Komura, K.; Sugi, Y. Fe(III) containing MCM-48 type mesoporous molecular sieves with framework zeolite secondary building units. *J. Nanosci. Nanotechnol.* **2008**, *8*, 400–404.
- (11) Parker, L. M.; Bibby, D. M.; Miller, I. J. Formation of ketenes by reaction of carboxylic acids over alkali metal-exchanged zeolites. *J. Catal.* **1991**, *129*, 438–446.
- (12) Gadhwal, S.; Dutta, M. P.; Boruah, A.; Prajapati, D.; Sandhu, J. S. Zeolite-HY: A selective and efficient catalyst for the synthesis of amides under microwave irradiation. *Ind. J. Chem., B* **1998**, *37B*, 725–727.
- (13) Huang, S. J.; Huang, C. H.; Chen, W. H.; Sun, X.; Zeng, X.; Lee, H. K.; Ripmeester, J. A.; Mou, C. Y.; Liu, S. B. Probing the alkyl ligands on silylated mesoporous MCM-41 using hyperpolarized ^{129}Xe NMR spectroscopy. *J. Phys. Chem., B* **2005**, *109*, 681–684.
- (14) Reddy, K. M.; Song, C. Synthesis of mesoporous molecular sieves: Influence of aluminum source on Al incorporation in MCM-41. *Catal. Lett.* **1996**, *36*, 103–109.
- (15) Sakthivel, A.; Dapurkar, S. E.; Gupta, N. M.; Selvam, P. The influence of aluminum sources on the acidic behaviour as well as on the catalytic activity of mesoporous H-AlMCM-41 molecular sieves. *Mesoporous Mesoporous Mater.* **2003**, *65*, 177–187.
- (16) Sing, K. S. W.; Everett, D. H.; Haul, R. A. W.; Moscow, L.; Pierotti, R. A.; Rouquerol, T.; Siemieniewska, T. Reporting physisorption data for gas/solid systems with special reference to the determination of surface area and porosity. *Pure Appl. Chem.* **1985**, *57*, 603–619.
- (17) Raftery, D.; Chmelka, B. F. In *NMR Basic Principles and Progress*; Bluemich, B., Kosfeld, R., Eds.; Springer-Verlag: Berlin, 1993; Vol. 30, pp 111–158.
- (18) Moudrakovski, I. L.; Terskikh, V. V.; Ratcliffe, C. I.; Ripmeester, J. A.; Wang, L. Q.; Shin, Y.; Exarhos, G. J. A ^{129}Xe NMR study of functionalized ordered mesoporous silica. *J. Phys. Chem., B* **2002**, *106*, 5938–5946.
- (19) Sakthivel, A.; Huang, S. J.; Chen, W. H.; Lan, Z. H.; Chen, K. H.; Kim, T. W.; Ryoo, R.; Chiang, A. S. T.; Liu, S. B. Replication of mesoporous aluminosilicate molecular sieves (RMMs) with zeolite framework from mesoporous carbons (CMKs). *Chem. Mater.* **2004**, *16*, 3168–3175.
- (20) Oka, H.; Kamioka, K.; Tokunaga, Y.; Okada, T. Solid state defects in calcined CaA zeolite. *Zeolites* **1997**, *19*, 455–457.
- (21) Montesinos-Castellanos, A.; Zepeda, T. A. High hydrogenation performance of the mesoporous NiMo/Al(Ti, Zr)-HMS catalysts. *Mesoporous Mesoporous Mater.* **2008**, *113*, 146–162.
- (22) Khodabandeh, S.; Davis, M. E. Synthesis of CIT-3: A calcium aluminosilicate with the heulandite topology. *Mesoporous Mater.* **1997**, *9*, 149–160.
- (23) Khodabandeh, S.; Davis, M. E. Alteration of perlite to calcium zeolites. *Mesoporous Mater.* **1997**, *9*, 161–172.
- (24) Beta, I. A.; Hunger, B.; Böhlmann, W.; Jobic, H. Dissociative adsorption of water in CaNaA zeolites studied by TG, DRIFTS, and ^1H and ^{27}Al MAS NMR spectroscopy. *Mesoporous Mesoporous Mater.* **2005**, *79*, 69–78.
- (25) Ryoo, R.; Jun, S.; Kim, J. M.; Kim, M. J. Generalized route to the preparation of mesoporous metallosilicates via post-synthetic metal implantation. *Chem. Commun.* **1997**, *22*, 2225–2226.
- (26) Miyamoto, Y.; Katada, N.; Niwa, M. Acidity of β zeolite with different Si/Al₂ ratio as measured by temperature programmed desorption of ammonia. *Mesoporous Mesoporous Mater.* **2000**, *40*, 271–281.
- (27) Okabe, K.; Matsuzaki, K.; Hagiwara, H. Hydrothermal synthesis of calcium silicate of ZSM-5 structure in alkali–metal–cation free conditions. *Bull. Chem. Soc. Jpn.* **1990**, *63*, 1552–1554.

*Received for review April 22, 2009**Revised manuscript received October 15, 2009**Accepted October 17, 2009*

IE900641U